OVERHEAD LINE CONDUCTORS

OVERHEAD LINES IN THE POWER INDUSTRY

Transmission and distribution of electric energy from generating power stations to consumers is usually accomplished through interconnected networks of overhead and underground power lines. The choice between these two basic types of transmission lines depends on such factors as cost, length of the line, reliability, power to be transferred, space constraints, and environmental impact. Overhead electric power lines have been used predominantly since the end of the nineteenth century. They continue to be the most economical form of transmission and distribution of electric energy.

The subject of overhead lines comprises many topics from electrical and mechanical engineering, materials science, physics, meteorology, optimization, computer applications, and others. An exhaustive treatment of overhead power lines as an integrated part of a power system is offered in Refs. 1–4. The reading list provides additional texts and representative papers which treat this subject in greater detail.

Overhead Versus Underground

The choice between overhead and underground power lines is somewhat similar to the choice between surface and underground public transportation systems. Because of lower installation and maintenance costs, overhead lines prevail in rural areas. In densely populated areas, space limitations make underground distribution economically feasible. In addition, underground cables are less likely to be damaged by traffic or construction accidents, which also makes them attractive for urban systems.

Overhead lines are usually used for long distance transmission (several hundred miles) because it requires higher voltages and heat dissipation capabilities. Higher voltages are used to increase the efficiency of power transfer. Although overhead lines are more susceptible to weather conditions and

Table 1. Standard System Voltages

Rating, kV	
Nominal	Maximum
34.5	36.5
46	48.3
69	72.5
115	121
138	145
161	169
230	242
345	362
500	550
765	800
1100	1200

a variety of additional hazards associated with human or animal activities, they are also much easier to repair. In an underground system, locating and repairing a faulty section of a buried power cable is complicated and time-consuming.

The recent rise in public interest in environmental and aesthetic issues prompted the trend toward underground installations. Where underground lines are not feasible, existing overhead lines are sometimes relocated or modified to be more compact and aesthetically appealing.

Types of Overhead Lines

Power lines are usually classified as transmission (high voltage) or distribution (low voltage) lines. An intermediate link is sometimes defined as a subtransmission type. Transmission lines, also referred to as a part of the bulk power supply, connect generating plants with major load centers. They are also used for interconnections between regional networks to transmit power in emergencies or during peak usage and for power exchange when it is economically advantageous. High level ac voltages, 138 kV and above, are used for transmission. The range 345 kV to 745 kV is called extra-high voltages (EHV). Voltages above that level fall into the category of ultra-high voltages (UHV). Subtransmission networks operate at 34.5 kV to 115 kV and connect bulk power supply with distribution substations.

Finally, distribution lines distribute power to the end user at voltages below 34.5 kV. Distribution networks are subdivided into primary and secondary distribution networks. Both overhead and underground conductors are used widely for this part of a power system.

The previous classification is not strict, and lines whose voltages are close to the borderline may be classified as either, depending on their function. The operating voltages, however, are standardized. Table 1 lists standard voltages used in the United States and some other countries as defined in ANSI/IEEE Standards (5,6).

Design and Construction

Castro (7,8) offers an overview of the concepts and practices regularly employed in transmission line construction and design. An IEEE Guide (9) extensively reviews recommendations and available literature on this subject.

CHOICE OF CONDUCTORS

The choice of conductor material, size, and configuration (single wire or bundle) significantly affects overhead line design. Hesterlee et al. (10) discuss advantages and disadvantages of several major types of conductors.

Materials

Overhead conductors are installed bare, covered with a weatherproof layer, or with electrical insulation. The metals for the conductor itself are copper, aluminum, steel, and combinations, such as aluminum conductor steel-reinforced (ACSR) and copper-clad steel. Table 2 lists the conductivity of these metals (adapted from (11)).

Conductor Materials

Copper. Copper has the highest electric conductivity among materials used for manufacturing of end products, surpassed only by silver and some rare metals. In combination with its mechanical properties and low cost, copper is the material of choice for a variety of electric applications. Copper, like many other metals, may be annealed to increase its mechancial strength and hardness. Based on the manufacturing process, three standard degrees of strength and hardness are distinguished: hard-drawn, medium-hard-drawn, and soft-drawn. Hard-drawn copper is used for long spans, medium-hard-drawn for shorter spans, and soft-drawn copper for short spans, connectors, taps, etc.

Aluminum. Aluminum is a widely available and inexpensive material, also commonly used for overhead transmission. In recent years, a gradual shift from copper to aluminum conductors occurred because of changes in availability and cost of both materials. The conductivity of aluminum is about 60% that of copper. Its specific gravity is only about one-third that of copper, and its tensile strength is comparable to that of the weakest, soft-drawn copper. Steel reinforced aluminum conductor (ACSR) has a high weight-to-strength ratio and high electrical conductivity. Other commonly used conductors include aluminum conductor alloy-reinforced (ACAR), all-aluminum conductor (AAC), and all-aluminum alloy conductor (AAAC).

Steel. Because of its high tensile strength, steel is commonly used to reinforce copper and aluminum conductors by wrapping strands of aluminum or copper wire around a central steel core or by using a solid nonstranded conductor. The steel core, which has relatively low conductivity, must be placed in the center, because the current density in the center of the cross section of a power line conductor is lower than the current density in the outer region. Such arrangement minimizes undesirable energy losses due to ohmic conduction.

Table 2. Conductivity of Various Metals

Material	Conductivity at 20 °C, MS/m
Aluminum	35.4
Copper, annealed	58.0
Copper, hard drawn	56.5
Iron, 99.98%	10.0
Gold, pure drawn	41.0
Silver	61.4
Steel, 99.98%	5 to 10

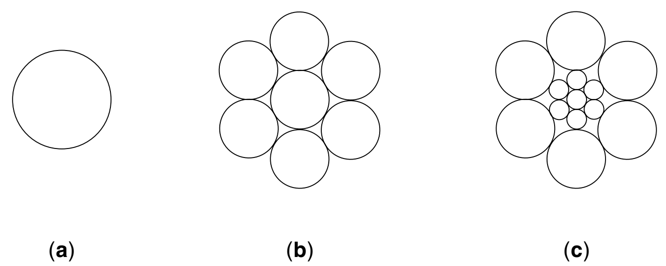

Figure 1. Conductor cross sections: (a) single-wire; (b) all aluminum conductor (AAC); (c) aluminum conductor steel reinforced (ASCR). Steel core increases conductor's tensile strength.

Figure 1 shows representative cross sections of several types of conductors.

Alloys. Various alloys are used in special cases to bring out the best properties provided by basic materials. Examples of copper alloys include cadmium copper, brass, and bronze. Usually, copper alloys have lower conductivity than copper, but higher mechanical strength. Aluminum alloys may sometimes be used as conductor cores instead of steel.

Conductor Coverings. Weatherproof coverings made of impregnated cotton, hemp, or rubber were used in previous years to prevent damage to conductors by tree limbs, weather, and other wires. Nowadays, overhead conductors are installed bare or are covered by plastic insulation, such as polyethylene or polyvinyl chloride (PVC).

Conductor Size

Economic Optimization. A variety of standard conductor sizes are available for all types of materials. The choice of conductor size depends on several considerations. Usually, the designer's goal is to minimize the overall cost as a function of conductor size while satisfying constraints posed by other factors, such as corona effects and mechanical stresses. Figure 2 illustrates this concept. As the diameter and, consequently, the weight of the conductor increases, the cost of the conductor itself combined with the cost of the support structures and installation labor increases as well. At the same time, larger diameter results in lower resistance (smaller heat dissipation power losses, higher power capacity) and lower voltage gradients in the vicinity of the conductor's surface (smaller power losses due to a corona).

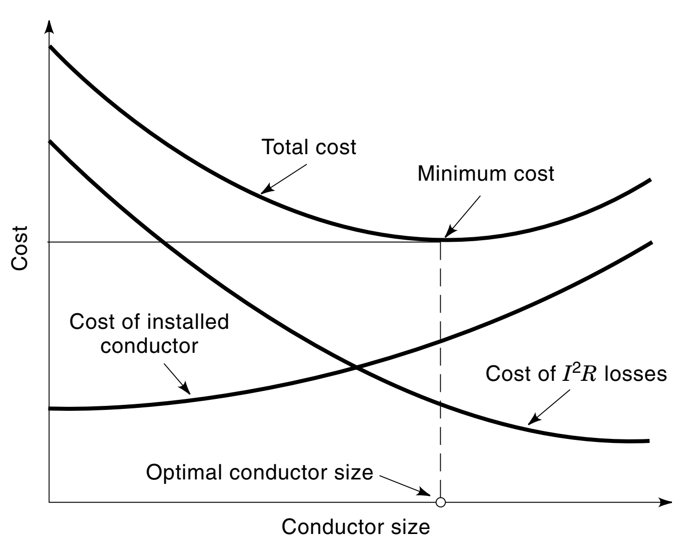

Figure 2. The choice of a conductor size is dictated by the total cost. Lower operating costs may justify high installation costs.

Usually, the sum of all costs forms a curve with a relatively flat region near the minimum. The designer can choose between a few acceptable options and optimize the design with respect to other factors, such as predicted market prices of raw materials.

Physical Effects. For voltages below 345 kV, the cost analysis is usually sufficient. However, for extra high voltage (EHV) transmission lines, the equivalent size of conductors may have to be increased to reduce excessive radio and audible noise produced by a corona. It may become advantageous to install a bundle of thinner conductors in place of a large single conductor. The advantages of the smaller diameter conductors are that they are easier to manufacture, transport, and install. Also, mechanical stress is distributed more evenly among support structures. Naturally, increasing the diameter of the conductor leads to heavier wind and ice loads. Reference 12 analyzes the wind-induced loads on overhead lines.

Ampacity. The maximum allowable current through an overhead conductor is limited by I^2R heating and the rate of heat loss. Standard practice suggests that the temperature of the conductor should be limited to 75°C. (The recent industry trend is toward higher temperatures.) Undesirable phenomena above this temperature include excessive sag increase, annealing, and change of mechanical and electrical properties. Unlike underground cable conductors, overhead conductors usually have sufficiently high heat loss rates due to a combination of convection and radiation. Reference 13 describes heating effects and their relationship to the current-carrying capacity of overhead conductors. Reference 14 is a generally accepted industry standard for calculating the ampacity of bare overhead conductors.

SAGGED CONDUCTORS

The dimensions of conductor sag are important for the design, maintenance, and computer simulation of overhead power lines. The requirements which must be satisfied during the design stage include minimum ground clearances and the mechanical strength of the supporting structures and the conductors themselves. Sag is inevitable. An infinite tension would be necessary to keep a horizontally suspended conductor perfectly straight. Various methods were developed to find the optimal dimensions of the sag for each application. In recent years, transition from manual techniques, such as those given by Thomas (15) and Martin (16), to computer programs has automated the design optimization of overhead lines.

Variation of the Conductor Length

Sag does not remain constant during the operation of an overhead line. The length of the conductor changes with its temperature, which depends on the weather conditions and also on the power losses in the conductor.

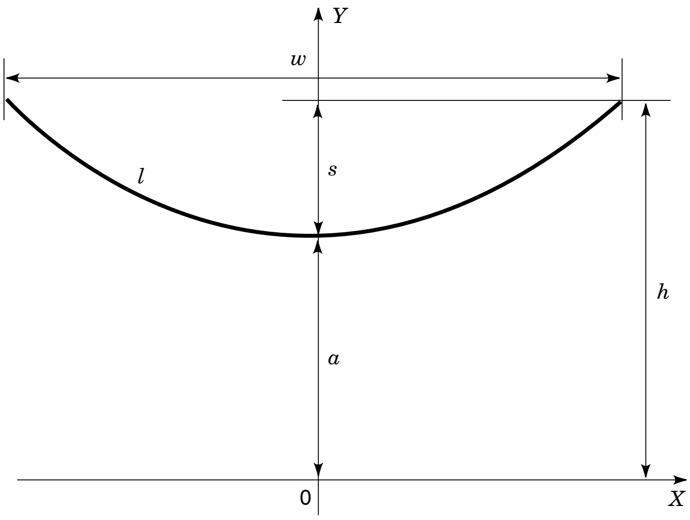

Figure 3. Mathematical representation of a sagged conductor is a catenary. It can also be closely approximated with a parabola.

In addition to thermal expansion and contraction, creep causes continuous elongation. Creep is an inelastic, irreversible stretch of conductors under applied tension which lasts for the entire lifetime of the conductor. The rate of elongation, however, substantially decreases with time. Aluminum conductors have the highest creep rates. The creep phenomenon has become important during the last forty years, when construction of tall towers with long spans became necessary because of higher transmission voltages.

Catenary Equations

Exact Equations. A suspended conductor assumes the shape of a catenary, also called a "chain curve," which is described by a hyperbolic cosine. Strictly speaking, the catenary is the shape of a perfectly flexible chain suspended by its ends and acted on by gravity. Its equation was obtained by Leibniz, Huygens, and Johann Bernoulli in 1691. Equations (1)–(3) provide the relationships for the geometric parameters shown in Fig. 3.

$$y = a\cosh\frac{x}{a} \tag{1}$$

$$s = a\left(\cosh\frac{x}{a} - 1\right) \tag{2}$$

and

$$l = 2a\sinh\frac{x}{a} = \sqrt{y^2 - a^2} \tag{3}$$

where l is the total length of the catenary of width $2x$. The height h of the point of suspension is equal to the sum of the sag s and the distance a from the lowest point to the origin. For sagged power line conductors, geometric origin (the point of intersection of the X and Y axes) is usually located far below ground level.

At the beginning of the century, Thomas (15) proposed a nondimensional representation of a catenary. The nondimensional unit-span basis representation is convenient because it reduces the number of independent geometric parameters. All conductors with the same ratio of sag s to span w are represented by the same unit curve. Bradbury (17) provides mathematical tools to analyze sags when the points of suspension are at unequal heights.

Parabolic Approximation. For all practical purposes, the sagged conductor may also be represented by a parabola. The first two terms of a power series expansion of Eq. (1)

$$y = a + \frac{1}{2!}\frac{x^2}{a} + \frac{1}{4!}\frac{x^4}{a^3} + \cdots \tag{4}$$

approximate Eq. (1) with an error of less than 2% for most spans encountered in the power industry. A widely used approximate equation relates sag s, span w, weight of the conductor F in kilograms per meter length, and the horizontal tension T in kilograms:

$$s = \frac{Fw^2}{8T} \tag{5}$$

In this case, linear dimensions are expressed in meters.

LIGHTNING PROTECTION

Two articles in this encyclopedia, Power system protection, and Lightning, lightning protection, and test standards, treat this topic in greater detail. A very brief overview of this complex subject is given here.

Lightning Discharge

Natural lightning may be intracloud, cloud-to-cloud, or cloud-to-ground. The latter represents the highest danger to electric power systems. A complete lightning discharge of any type is called a flash. Uman (18) comprehensively analyzes the types of lightning flashes and discusses associated physical and mathematical models.

A standard lightning impulse waveform has been accepted internationally to facilitate comparison of results in disparate areas of research. A standard impulse has a front time of 1.2 μs and time half value of 50 μs. It is easily generated under laboratory conditions.

Overvoltages

Lightning flashes result in severe overvoltages, leading to insulation breakdown of connected power equipment, and thus are considered to be highly undesirable. More frequently, lightning causes temporary faults, usually cleared by protective equipment in a matter of seconds. Twenty years ago such momentary interruptions of the power supply were acceptable, but nowadays increasingly sophisticated equipment is so sensitive to interruptions that preventing them is a major design goal.

Lightning Performance

Lightning causes flashovers from direct strokes or from nearby strokes. Even if lightning does not hit a line directly, the voltages induced in the line conductors by the lighting discharge may be significant enough to interrupt normal operation mode. Induced voltage surges are generally much lower than those caused by a direct strike. The insulation clearances of transmission lines are usually sufficient to withstand induced voltage surges, whereas distribution lines are much more vulnerable. Reference 19 describes the details of the lightning performance evaluation.

Shield Wires. A standard way of enhancing the lightning protection of overhead lines is to place a shield wire above the phase conductors. The shield intercepts direct lightning strokes into the phase conductors and provides a conduction path for the lightning current to the ground. The effectiveness of the shield wire is limited because the lightning surge current increases the local potential of the ground lead to levels that may be sufficiently high to cause a back flashover to the phase conductors.

Arresters. Distribution arresters of various types are widely used to protect power equipment and line insulation. The arrester has high impedance at normal operating voltages and low impedance under high voltage conditions caused by the lightning surge. Many different types of arresters and varistors were developed over the last few decades. The ANSI/IEEE Standard (20) provides specific characteristics of widely used intermediate-class arresters.

CORONA

Mechanism of Discharge

Corona discharges appear around overhead conductors when the intensity of the electric field in the immediate vicinity of the conductor exceeds the breakdown strength of air (30 kV/cm under normal conditions). These discharges do not normally lead to flashovers between conductors and/or ground because the electric field intensity falls off as the distance from the conductor increases. The breakdown strength of air is a function of several variables including pressure, humidity, type of voltage (ac or dc), and photoionization. The distribution of the local electric field near the surface of a conductor depends on surface irregularities caused by droplets of water, contaminant particles, and local mechanical stresses on the conductor itself.

At first, it may seem counterintuitive that newly strung conductors have higher corona losses and noise than the aged conductors do. The corona effects decrease, thus improving the overall performance of the transmission line, because the surface of the conductor becomes smoother with time. The intensity of the electric field is higher near sharp irregularities, which become the sources of a corona when the transmission line is designed just below the threshold of corona discharge. Local ion bombardment in the electric field enhancement regions, combined with weather impact and continuously applied tension, gradually smooth out sharp spikes of metal, bird droppings, and any other irregularities at the surface. Preconditioning of the surface by sandblasting reduces corona effects in new conductors by the same mechanism.

Increase in the conductor diameter decreases the electric field at the conductor surface thereby decreasing the corona discharges. In some cases, the size of the conductor suggested by the voltage rating of a power line may significantly exceed that required by the current-carrying capacity.

Corona Effects

Audible Noise. The audible noise of high-voltage ac transmission is sometimes significant enough to require variation of the line design parameters. The noise reaches its highest levels during or immediately after rain. The standard measurement procedures of transmission line audible noise are based on the A-weighted sound level measured during rain and averaged over a considerable period of time (usually 1 year). Indices L_{50} and L_5 denote the level exceeded correspondingly 50% or 5% of the time during rain. Also, the average level (close to L_{50} value) and heavy rain level (close to L_5 value) are considered.

Statistical studies show that complaints regarding excessive noise begin when it reaches 50 to 55 dB(A) above the reference sound pressure of 20 μPa at 30 m distance from the power line. The units dB(A) refer to the A-weighting network used by sound-measuring instruments. This type of network emphasizes the importance of frequencies in the 1 kHz to 5 kHz range, because these are the frequencies at which the human ear is most sensitive. Although audible noise levels are higher during the rain, the complaints are more numerous after rain, because the sound of the rain itself masks the corona noise. For this reason, regulations usually refer to fair weather conditions.

Radio and TV Noise. Although radio-frequency interference is produced by corona discharges, it is usually below levels which noticeably interfere with broadcast and communication equipment. Significant interference is a sign of malfunctioning insulation, typically, due to contamination of the line insulators or degraded performance of line hardware. Proper installation and maintenance procedures prevent excessive radio-frequency interference. As with audible noise, the levels of radio-frequency noise vary with weather.

Corona Loss. Each of the corona-related phenomena, whether audible or radio noise, glow or heat, requires a certain amount of energy. The total power per mile dissipated by these phenomena on a typical EHV transmission line varies from several kilowatts in fair weather to hundreds of kilowatts in foul weather. Although these losses are usually smaller than the I^2R power dissipation, they still must be accounted for during the line planning and design stage. As transmission voltages increase, the corona loss requirements are usually satisfied automatically after acceptable reduction of the audible and radio noises.

ELECTRIC AND MAGNETIC FIELDS

Basic Concepts and Definitions

Units. The electric field, defined through the gradient of electric potential as $\boldsymbol{E} = -\nabla\Phi$, has units of V/m. The magnetic field in the vicinity of power lines is usually measured in terms of the magnetic flux density $\boldsymbol{B}$, which has units of tesla (T), rather than in terms of the magnetic field strength $\boldsymbol{H} = \boldsymbol{B}/\mu_0$ (the units of $\boldsymbol{H}$ are A/m). A commonly used unit for $\boldsymbol{B}$ is gauss (G). One gauss is equal to 10^{-4} T, and $\mu_0 = 4\pi \cdot 10^{-7}$ H/m is the permeability of free space.

Vector Fields. Both electric and magnetic fields are vector fields, which means that their instantaneous value at each

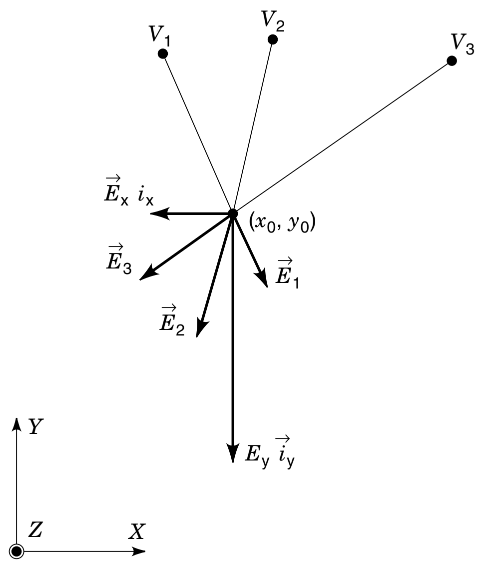

Figure 4. The sum of all electric field vectors at each point in space can be divided into orthogonal field components.

point in space is described by the magnitude and direction of the field vector:

$$\boldsymbol{E} = e_x(t)\boldsymbol{i}_x + e_y(t)\boldsymbol{i}_y + e_z(t)\boldsymbol{i}_z \tag{6}$$

For sinusoidal steady-state fields at radian frequency ω, each space component is defined by the magnitude E_i and the phase angle ϕ_i:

$$e_i(t) = E_i \cos(\omega t + \phi_i) \tag{7}$$

Harmonic Content. Harmonic is a component frequency of a periodic signal that is an integral multiple of the fundamental frequency. A pure sinusoidal signal contains only a fundamental harmonic. Currents and voltages on transmission line conductors usually contain a certain amount of higher harmonics, indicated by the magnitude and order of the Fourier series terms describing the signal.

Superposition. Because we consider aerial power lines and air is a linear dielectric, the principle of superposition applies: if several field sources are present in the vicinity of a certain point in space, the resultant field at this point is the sum of the fields created by each of these sources independently. The superposition principle helps to understand the origin of the rotation of field vectors.

Figure 4 shows a cross-sectional view of three energized conductors in the vicinity of the observation point (x_0, y_0). Superposition suggests that, at each moment, the electric field generated by each of these conductors depends on the instantaneous value of the voltage at each conductor.

Calculation Methods

Electric Fields. The most commonly used method for finding electric fields generated by power line conductors is first to compute the charges on the lines assuming a two-dimensional geometric arrangement, where conductors are considered infinitely long, parallel cylinders above perfectly conducting, flat ground.

The approximating assumption of a perfectly conducting soil is justified by comparing its relaxation time to one period of 60 Hz power frequency. For most types of soils, the relaxation time $\tau = \epsilon/\sigma$ ranges from milliseconds to nanoseconds, whereas the duration of the power frequency period is $\frac{1}{60}$ s $\approx$ 17 ms. Both theoretical and empirical correction factors are sometimes introduced to account for this approximation.

Assuming that no free charge is in the air, the distribution of the electric potential Φ in the vicinity of an overhead power line obeys Laplace's equation:

$$\nabla^2\Phi = 0 \tag{8}$$

The solution for the straight infinite conductor of zero radius in free space with charge per unit length q takes the form

$$\Phi = -\frac{q}{2\pi\epsilon_0}\ln\frac{r}{r_0} \tag{9}$$

where the permittivity constant $\epsilon_0 \approx 8.854 \cdot 10^{-12}$ F/m, r_0 is the arbitrary reference position of zero potential, and r is the position of the observation point, expressed in rectangular coordinates as

$$r = \sqrt{(x-x')^2 + (y-y')^2} \tag{10}$$

Figure 5 shows the coordinate system used in this analysis.

According to image theory, the currents in perfectly conducting flat ground are accounted for by adding a line charge of opposite polarity placed symmetrically with respect to the ground-air boundary. When the ground is taken into account, the potential distribution in the upper plane obeys the following relationships:

$$\Phi = -\frac{q}{2\pi\epsilon_0}\ln\frac{r}{r^i} \tag{11}$$

and

$$r^i = \sqrt{(x-x')^2 + (y+y')^2} \tag{12}$$

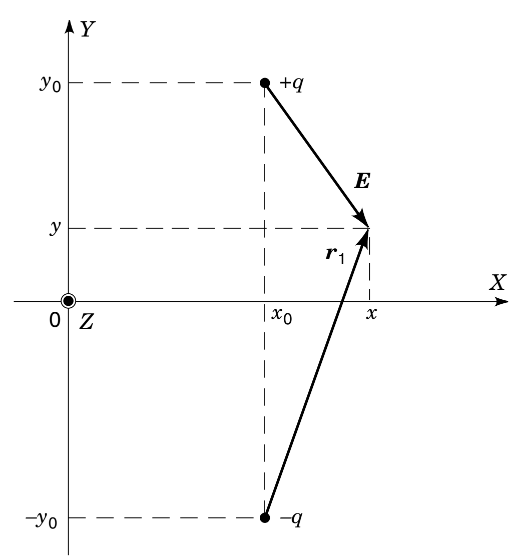

Figure 5. Two parallel line charges of opposite polarity at a distance $2y_0$ apart illustrate image theory principles.

where r^i is the distance from the image charge to the observation point. Now, we can consider the potential of an infinite conducting cylinder of small radius r_a. Because the wires are considered to be perfectly conducting, the potential Φ' at the surface of the wire of radius r_a is assumed to be known:

$$\Phi' \approx -\frac{q}{2\pi\epsilon_0}\ln\frac{r}{2y_0} \tag{13}$$

where q is the total charge per unit length. Solving for the charge q,

$$q = -\left(\frac{2\pi\epsilon_0}{\ln\dfrac{r}{2y_0}}\right)\Phi' \tag{14}$$

where the term in parentheses has units of capacitance per unit length and, in fact, represents the capacitance per unit length between the conductor and earth.

Similar analysis applies for the case of multiple parallel conductors. Suppose that there are N lines and it is assumed that the potential known at the surface of the m'th line:

$$\Phi_m = -\sum_{n=1}^{N}\frac{q_n}{2\pi\epsilon_0}\ln\frac{r_{mn}}{r^i_{mn}} \tag{15}$$

$$r_{mn} = \sqrt{(x_m - x_n)^2 + (y_m - y_n)^2} \tag{16}$$

and

$$r^i_{mn} = \sqrt{(x_m - x_n)^2 + (y_m + y_n)^2} \tag{17}$$

Thereby, the potential on each wire is described by a matrix equation

$$[\Phi] = [P][Q] \tag{18}$$

where the entries of the matrix $[P]$ are called Maxwell potential coefficients. Each conductor is characterized by a phasor potential with real and imaginary components $\Phi = \Phi_r + j\Phi_i$.

Solving for the real $[Q_r]$ and imaginary $[Q_i]$ charges separately, we obtain two separate matrix equations:

$$[Q_r] = [P]^{-1}[\Phi_r] \tag{19}$$

and

$$[Q_i] = [P]^{-1}[\Phi_i] \tag{20}$$

The diagonal entries of the $[P]$ matrix are seen from Eq. (14):

$$P_{nn} = \frac{1}{2\pi\epsilon_0}\ln\left(\frac{2y_a}{r_a}\right) \tag{21}$$

where r_a is the radius of the conductor a, and the off-diagonal entries are easily derived from Eqs. (15)–(17):

$$P_{mn} = \frac{1}{2\pi\epsilon_0}\ln\left[\sqrt{\frac{(x_m - x_n)^2 + (y_m + y_n)^2}{(x_m - x_n)^2 + (y_m - y_n)^2}}\right] \tag{22}$$

For this approximate analysis, it is assumed that the conductors have a finite radius when the diagonal term is calculated. However, when the off-diagonal terms are found, the conductors are represented as line charges. This assumption is valid for overhead lines because the diameter of each wire is orders of magnitude smaller than the distance to the ground and to the distances between conductors. Zahn (21) provides a precise solution to this problem, where the distances used in Eqs. (15)–(22) are not between the centers of conductors, but slightly offset because of interaction between the charges.

Because our purpose is to find the electric field distribution, we take the spatial gradient of the potential:

$$\boldsymbol{E} = -\nabla\Phi \tag{23}$$

which, after substitution of Eq. (15) in Eq. (23), finally produces a representation of the electric field, as determined by the charges found from Eqs. (19) and (20):

$$\begin{aligned}\boldsymbol{E} = \sum_{n=1}^{N}\frac{q_{r,n} + jq_{i,n}}{2\pi\epsilon_0}\Bigg[&\left(\frac{x - x_n}{r_n^2} - \frac{x - x_n}{(r^i_n)^2}\right)\boldsymbol{i}_x \\ &+ \left(\frac{y - y_n}{r_n^2} - \frac{y + y_n}{(r^i_n)^2}\right)\boldsymbol{i}_y\Bigg]\end{aligned} \tag{24}$$

Assuming a simple earth model (an ideally flat medium of infinite conductance), the previous expression simplifies considerably for fields at ground level. At points of zero height ($y = 0$), the electric field vector is vertical, which follows from Eq. (24) and agrees with the boundary condition requiring a zero tangential electric field component at the surface of a perfect conductor. In this case, Eq. (24) simplifies to

$$E_y(y = 0) = -\sum_{n=1}^{N}\frac{q_{r,n} + jq_{i,n}}{2\pi\epsilon_0}\frac{2y_n}{(x - x_n)^2 + y_n^2} \tag{25}$$

The previous analysis holds approximately for bundle conductors when the fields are calculated sufficiently far from the bundle. Then, the geometric mean radius (GMR), multiplied by two, is used instead of the diameter of the phase conductor:

$$\mathrm{GMR} = \frac{D}{2}\sqrt[n]{\frac{nd}{D}} \tag{26}$$

where n is the number of subconductors, d is the diameter of each individual subconductor, and D is the bundle diameter.

Pages 332–335 of Ref. (1) provide generalized curves for computing the electric fields at ground level produced by simple single-circuit configurations. These curves help to analyze the effects of line height, conductor size, sag, and phase spacing.

Magnetic Fields

Ampère's Law. Ampère's law relates the magnetic field intensity $\boldsymbol{H}$ to its source, the current density $\boldsymbol{J}$, and the time-changing electric field $\boldsymbol{E}$ by

$$\oint_C \boldsymbol{H}\cdot d\boldsymbol{l} = \int_S \boldsymbol{J}\cdot d\boldsymbol{S} + \frac{d}{dt}\int_S \epsilon_0\boldsymbol{E}\cdot d\boldsymbol{S} \tag{27}$$

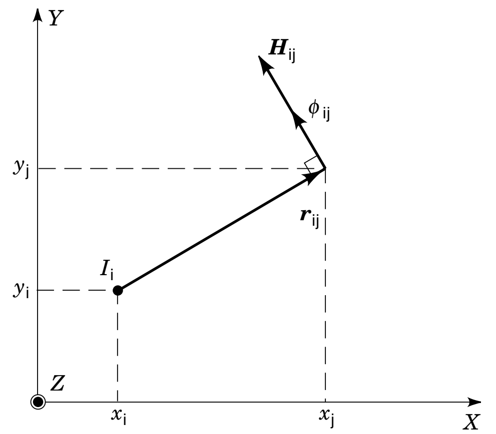

Figure 6. Magnetic field produced at the observation point (x_j, y_j) by a line current I_i.

In the magneto-quasi-static approximation, the time derivative of the electric field $\boldsymbol{E}$ is negligible. Then, the magnetic field produced by an infinitely long uniform line current I_i flowing in the positive z direction using the coordinate system shown in Fig. 6 is given by

$$\boldsymbol{H}_{j,i} = \frac{I_i}{2\pi r_{i,j}} \boldsymbol{\phi}_{i,j} \tag{28}$$

where $\boldsymbol{\phi}_{i,j}$ is the unit vector in the direction of the cross-product of the current vector and the vector $\mathbf{r}_{i,j}$. In rectangular coordinates, the unit vector $\boldsymbol{\phi}_{i,j}$ is expressed by the unit vectors in the direction of the horizontal and vertical axes, $\boldsymbol{i}_x$ and $\boldsymbol{i}_y$:

$$\boldsymbol{\phi}_{i,j} = \frac{y_i - y_j}{r_{ij}} \boldsymbol{i}_x - \frac{x_i - x_j}{r_{ij}} \boldsymbol{i}_y \tag{29}$$

By superposition, the total magnetic field at the observation point (x_j, y_j) is the sum of contributions of magnetic fields from each current:

$$\boldsymbol{H}_j = \sum_i \frac{I_i}{2\pi r_{ij}} \left(\frac{y_i - y_j}{r_{ij}} \boldsymbol{i}_x - \frac{x_i - x_j}{r_{ij}} \boldsymbol{i}_y \right) \tag{30}$$

The magnetic flux density is given by

$$\boldsymbol{B} = \mu_0 \boldsymbol{H} \tag{31}$$

where $\mu_0 = 4\pi \cdot 10^{-7}$ H/m is the permeability of free space.

The previous model is the simplest possible. It assumes no earth, straight, infinitely long, thin conductors, no coupling of electric and magnetic fields, (quasi-static approximation), and no shielding objects in the vicinity of the observation point. Nevertheless, the model is adequate for most purposes. More complicated models are treated in detail in research work published over the last century.

Carson (22) and, later, Krakowski (23) proposed techniques to account for the earth return currents. Modified versions of Carson's approach are extensively used in computational models. The relative contribution of the ground currents usually increases with the distance from the overhead line.

Biot–Savart Law. Alternatively, the Biot–Savart law may be used instead of Ampère's law to compute magnetic field intensity:

$$\boldsymbol{H} = \frac{1}{4\pi} \int_{V'} \frac{\boldsymbol{J}(r') \times \boldsymbol{i}_{rr'}}{|\boldsymbol{r} - \boldsymbol{r}'|^2} dv' \tag{32}$$

and

$$\hat{\boldsymbol{H}} = \frac{1}{4\pi} \int_{l} \frac{\hat{I} d\boldsymbol{l} \times \boldsymbol{i}_{rr'}}{|\vec{r} - \vec{r}'|^2} \tag{33}$$

where $\boldsymbol{i}_{rr'}$ is the unit vector in the direction of $\boldsymbol{r}_{ij}$ and the "ˆ" sign indicates a sinusoidal change in time. It is a matter of taste and practicality, which set of equations to use.

Rotation of the Field Vector

Quasi-Static Approximation. The elliptical rotation of the field vectors takes place when several field sources driven at the fundamental frequency are present, the locations of these sources and the observation point cannot be connected with a single straight line, and a phase difference between the sources exists (as it happens in multiphase conductor arrangements). We can easily illustrate this concept with a two-dimensional approximation, and the results are easily generalized to three dimensions. We use the magnetic field as an example, but this discussion also applies to electric fields.

For most regions in the vicinity of a power line, we approximate overhead conductors as straight, infinitely long, parallel wires to which an ac sinusoidal voltage is applied. Because the wavelength of the electromagnetic field at the 60 Hz power frequency is around 5000 km, the voltage and the current levels are practically the same for the part of the conductor which noticeably contributes to the field. Under these conditions, we describe the field distribution with a two-dimensional model, assuming that the fields do not change in the z direction, as indicated in Fig. 6.

Lissajous Figures. As indicated in Eq. (30), the vector contributions from each current can be added up. A simple trigonometric manipulation applied to the field vectors along each orthogonal direction shows that the sum of sinusoidal signals of a single frequency adds up to a sinusoid of the same frequency whose magnitude and phase depend on the individual components of the signal.

Two sinusoidal signals applied in two orthogonal directions form a Lissajous figure whose exact shape depends on the magnitude and phase of each orthogonal component. In general, the shape of a Lissajous figure formed by two single-frequency orthogonal signals is an ellipse. Two special cases exist:

1. When the phase angle between the two components is either 0° or 180°, the ellipse degenerates into a straight line.
2. When the phase angle is ±90° *and* the magnitudes of the orthogonal components are equal to each other, the semimajor and semiminor axes of the ellipse are equal, and the ellipse becomes a circle.

Maximum and Resultant Field. Because the tip of the magnetic field vector in the vicinity of a power line generally traces an elliptical path, there is more than one way to quantify the level of the magnetic field. The concepts of maximum and resultant field values are normally used.

Suppose that, at a given point in space, the superposition of the magnetic fields produced by all present sources adds up to the orthogonal components H_x and H_y of the magnetic field vector of certain magnitude H and phase θ:

$$h_x(t) = H_x \cos(\omega t + \theta_x) \tag{34}$$

and

$$h_y(t) = H_y \cos(\omega t + \theta_y) \tag{35}$$

The resultant field is defined as an rms value of the vector sum of $h_x(t)$ and $h_y(t)$:

$$H_{\mathrm{R}} = \sqrt{\frac{1}{T}\int_0^T ([h_x(t)]^2 + [h_y(t)]^2)\,dt} \tag{36}$$

where T is the period of magnetic field oscillation. The maximum field is defined as

$$H_{\mathrm{M}} = \sqrt{\frac{1}{T}\int_0^T \left(\sqrt{[h_x(t)]^2 + [h_y(t)]^2}\cos\alpha\right) dt} \tag{37}$$

where α is the angle between the rotating instantaneous field vector and the semimajor axis of the ellipse. Figure 7 visualizes the rotating field vector. One can measure the maximum field by a single-axis magnetic field meter aligned with the semimajor axis. To measure the resultant field, one has to know all Cartesian components, so, two (or three for a three-dimensional case) single-axis field probes are necessary. Comparing Eqs. (36) and (37) shows that the largest possible difference between the values of the maximum and the resultant fields is $\sqrt{2}$. If we define the minimum field as the magnitude of the field vector along the semiminor axis of the ellipse, then all possible values of the minimum field fall into the range between zero and the maximum field value.

Given the axial components of the field, the values of the maximum and minimum field can be found analytically. Because the instantaneous value of the field vector does not change when the vector goes through the point of its maximum or minimum, we can search for the solution of the following equation:

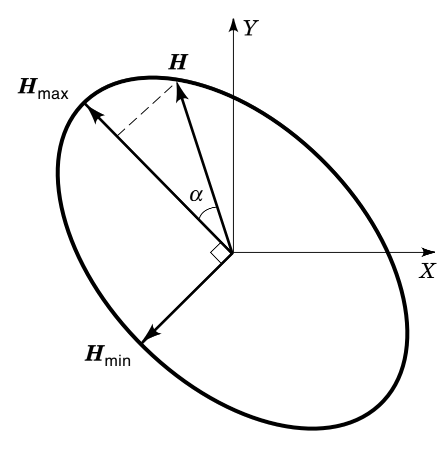

Figure 7. The tip of the magnetic field vector traces an elliptical trajectory in the vicinity of multiple sources.

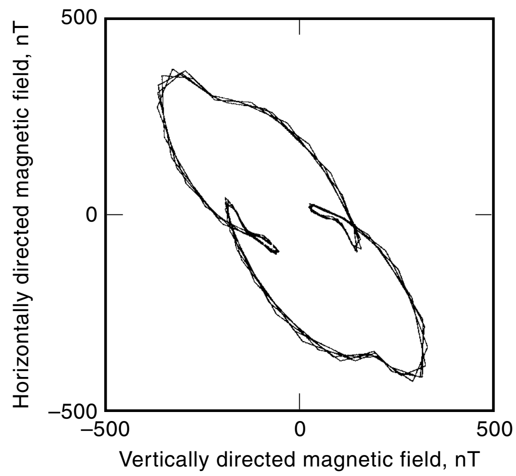

Figure 8. The presence of higher harmonics in the conductor currents distorts the shape of the trajectory traced by the tip of the magnetic field vector.

$$\frac{d}{dt}(H^2) = 0 \tag{38}$$

where H^2 is the sum of the squares of axial components. One solution to Eq. (38) is given by

$$\omega t = \frac{1}{2}\arctan\left(-\frac{H_x^2 \sin 2\theta_x + H_y^2 \sin 2\theta_y}{H_x^2 \cos 2\theta_x + H_y^2 \cos 2\theta_y}\right) \tag{39}$$

In general, there are four solutions to Eq. (38), two for each axis of the ellipse:

$$\omega t_m = \omega t_1 + (m-1)\frac{\pi}{2} \tag{40}$$

where m = 1, 2, 3, 4. The magnitudes of the semiaxes are found by substituting the solutions given by Eq. (40) in Eqs. (34) and (35) and taking the square root of the squares of each component.

Harmonic Content. As a rule, the currents and voltages in transmission line conductors have a certain fraction of higher frequency harmonics. Usually, the third harmonic has the highest magnitude. In this case, the shape of the rotating vector trajectory departs from the ideal ellipse. Figure 8 (24) shows the trajectory of a magnetic field vector near a 12.5 kV three-phase distribution power line. In this case, the magnetic field recorder with three orthogonal coils is reconstructed and visualized to show the effects of the high harmonic content. In many cases, however, these effects can be ignored, and the field can be characterized by the fundamental frequency.

Measurement Techniques

Most of the measurements of the electric and magnetic field environments were prompted by health concerns or by the need to manage induced currents and voltages in the objects on the ground. Randa et al. (25) provide an extensive inventory of published measurements of electromagnetic environments, in particular, for the frequency band 30 Hz to 300 Hz.

Field Perturbations and Variations

Unperturbed Fields. The fields produced by overhead lines are normally characterized by the values of the unperturbed fields in specific locations in the vicinity of the line, that is, the influence of the measurement equipment or any other objects in the vicinity of the measurement point should be minimized. Most objects are nonmagnetic. They strongly influence the spatial distribution of the electric field, whereas the magnetic field remains practically unchanged in their presence. Any conducting object, including the human operator of the equipment, should be removed from the electric field meter as far as about three times its largest linear dimension.

Temporal Variation. Determined by the line design specifications, the magnitudes of the voltages on the conductors vary only within about 10% from the nominal value. Consequently, the unperturbed electric field does not significantly change with time. The picture is very different for the magnetic field. The magnetic field depends on the currents in the conductors, which vary with the load demand from the consumer. In peak load conditions, such as summer time air-conditioning, for example, the currents and, consequently, the ambient magnetic field may be several times larger than the low value.

Lateral and Longitudinal Profiles. Of the entire three-dimensional spatial distribution of ambient overhead line fields, the fields at ground level are of the highest interest, because interaction with objects near the ground is most common. The field-mapping procedures, described by the IEEE Standard (26), require measurements in two directions, one perpendicular to the power line and one parallel to the power line, called the lateral and longitudinal profiles, respectively.

The lateral profile is usually taken at the lowest point of the conductor catenary. Figure 9 shows a typical shape of the lateral profile taken for the distribution level overhead line. The longitudinal profile is needed to characterize the influence of the conductors' sag, tower structures, and so on. The variation of field values along the longitudinal profile is usually smaller, and the measurement is taken at the coordinate of the highest field of the lateral profile.

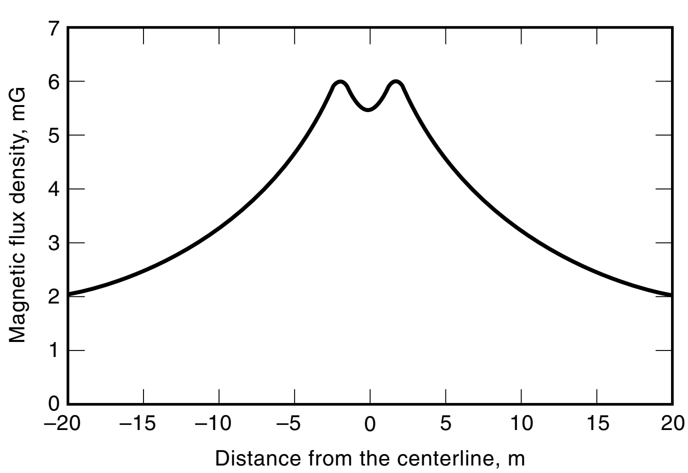

Figure 9. Lateral profile of the magnetic flux density at ground level under the 12.5 kV three-phase distribution power line. The conductors are at −1.1, 0, and 1.1 m from the centerline, about 9 m above the ground.

Meters

Electric Field. Two types of ac electric field meters designed specifically for measuring power line fields are described by (27,28). The first type is the free-body meter, which measures the steady-state current induced between two insulated conductors, and the second is the ground-to-reference type, which measures the current between the flat probe and the ground. The free-body meter is more commonly used because it is portable and does not require a ground reference. A single-axis meter is sufficient, because the electric field is usually nearly perpendicular at a standard 1 m height above the ground. Several brands of such meters are available commercially.

Magnetic Field. A variety of commercial magnetic field meters suitable for measuring extremely low frequency (ELF) magnetic fields produced by power lines are also readily available. As explained in the section entitled "Rotation of the Field Vector," the single-axis probes measure the maximum magnetic field (being properly oriented in space), and the three-axis meters measure the resultant field. Additional features include measuring the cumulative exposure over a period of time, recording capabilities for the field mapping measurements, computer interfacing, and ability to measure harmonic contents.

In most cases, magnetic field probes consist of electrically shielded wire coils which generate an electromotive force (emf) in response to changing magnetic flux. A planar conducting loop of area A placed in a quasi-static uniform sinusoidal magnetic field $\boldsymbol{H}(t) = H\ \sin(\cot)$ with the magnitude H and frequency ω generates an emf equal to

$$\text{emf} = -\omega\mu_0 HA\cos\omega t \tag{41}$$

assuming that the environment is nonmagnetic and that the direction of the H-field is orthogonal to the plane of the loop.

Calibration. The IEEE Standard (26) provides procedures for calibrating ELF electric and magnetic field meters. The magnetic field meters are calibrated by placing the sensor in a nearly uniform linearly polarized field of known magnitude and direction. Weber (29) gives the following rms value of the magnetic flux density B, expressed in gauss, at the center of a square loop of ac current with N turns and a side length of $2s$ meters:

$$B = \mu_0 \frac{\sqrt{2}IN}{\pi s} \cdot 10^{-4} \tag{42}$$

where I is the rms current in amperes.

Electric field calibration is done in several ways. For direct calibration, a uniform electric field is created by parallel plate electrodes or by a conducting plate with a guard ring placed under a high voltage line.

Field Effects

Health Concerns. Since the late sixties, the possible health hazards of power line electric fields were widely discussed and studied in several countries, including the United States, the Soviet Union, Sweden, and others. After the publication of the epidemiological study of childhood leukemia by (30), attention

Table 3. Likely Range of Maximum Vertical Electric Field Under Transmission Lines

Line Voltage, kV	Near-Ground Vertical Electric Field, kV/m
69	1 to 1.5
115	1 to 2
138	2 to 3
161	2 to 3
230	2 to 3.5
345	4 to 6
500	5 to 9
765	8 to 13

gradually shifted from electric to magnetic fields. A great deal of research was sponsored afterward by the government and the power industry. At this moment, no compelling evidence has been found that electric or magnetic fields produced by the overhead lines cause negative health effects. Although most scientists agree that some biological effects are induced by a magnetic field, it is not clear at what magnitude the power frequency field becomes hazardous and whether such levels are generated by typical installations.

Electromagnetic Induction and Interference. The effects of electric and magnetic fields are important regardless of the health hazards discussion. Various phenomena associated with electromagnetic induction and interference occur near a transmission line. Among the most noticeable are voltages and currents induced in gas pipelines, fences, vehicles parked under power lines, etc. Sunde (31) analyzes lightning-induced voltages and electromagnetic interference of power line fields with telephone and railroad systems. Electromagnetic compatibility issues often come in play. For example, power frequency magnetic fields interfere with cathode-ray tubes, which necessitates intricate magnetic field shielding. The magnetic field coupling is usually strong when objects on the ground run parallel to the overhead line (e.g., pipelines and fences), whereas the electric field is of concern when compact objects are considered.

Typical Field Values. The electric field at ground level increases with increasing line voltage. For 12 kV distribution lines, the typical electric field value is on the order of 10 V/m, and, for 765 kV lines, it is on the order of 10 kV/m. Common domestic appliances produce electric fields on the order of tens of volts per meter. Table 3 lists likely ranges of the electric field magnitude under transmission lines.

Magnetic fields cannot be specified equally well, because they depend on the load at a specific time. Typical measured values at ground level under distribution lines usually fall into the range of 1 to 10 mG, and, in a transmission line corridor, they are usually on the order of tens of mG. Household levels usually vary from 10 to 100 mG.

Minimization of Ambient Fields

The most common way of reducing ambient fields is to change some geometrical parameters of the line. Increasing line height is an obvious modification, because both electric and magnetic fields die away with the distance. This is done by building taller support structures or by placing them closer to each other to reduce conductor sag. However, this design strategy leads to higher construction costs.

Fields are partially canceled by changing the phase spacing. In this case, the analysis of the superposition of the fields due to each conductor reveals relatively simple techniques. For example, the field produced by a balanced three-phase delta configuration (wires form a triangle in the cross section) decays faster with distance than that of the flat configuration. The vertical configuration has lower fields far from the line than the flat configuration, etc. Even more effective field cancellation is achieved by phase splitting and arranging conductors in highly symmetrical patterns. The hexagonal pattern is most frequently proposed.

Construction of an inductively coupled loop near a transmission line, passive, as proposed by (32), or actively driven, as described by (33) helps to mitigate fields by careful placement of cancellation sources. These and other techniques, usually used in combination, reduce electric and magnetic fields below the maximum levels specified by local regulations. The standards for the levels used vary, and an individual approach is usually needed for each field management case. Additional discussion of field minimization techniques is in (34,35,36).

BIBLIOGRAPHY

1. *Transmission Line Reference Book: 345 kV and Above,* 2nd ed., Palo Alto, CA: Electric Power Research Institute, 1987.
2. D. G. Fink and H. W. Beaty (eds.), *Standard Handbook for Electrical Engineering,* 13th ed. New York: McGraw-Hill, 1993.
3. E. B. Kurtz and T. M. Shoemaker, *The Lineman's and Cableman's Handbook,* 6th ed., New York: McGraw-Hill, 1981.
4. G. R. Jones, M. A. Laughton, and M. G. Say (eds.), *Electrical Engineer's Reference Book,* 15th ed., London: Butterworth-Heinemann, 1993.
5. *Electric Power Systems and Equipment Voltage Ratings (60 Hertz),* ANSI/IEEE Standard C84.1, New York: American National Standards Institute, 1995.
6. *Preferred Voltage Ratings for Alternating-Current Electrical Systems and Equipment Operating at Voltages above 230 kV Nominal,* ANSI/IEEE Standard 1312, New York: American National Standards Institute, 1993.
7. R. D. Castro, Overview of the transmission line construction process, *Electr. Power Syst. Res.,* **35**: 119–125, 1995.
8. R. D. Castro, Overview of the transmission line design process, *Electr. Power Syst. Res.,* **35**: 109–118, 1995.
9. *IEEE Guide to the Installation of Overhead Transmission Line Conductors,* IEEE Std. 524-1992, New York: IEEE, 1992.
10. J. M. Hesterlee, E. T. Sanders, and F. R. Thrash, Jr., Bare overhead transmission and distribution conductor design overview, *IEEE Trans. Ind. Appl.,* **32**: 709–13, 1996.
11. H. A. Haus and J. R. Melcher, *Electromagnetic Fields and Energy,* Englewood Cliffs, NJ: Prentice-Hall, 1989.
12. *Transmission Line Reference Book: Wind Induced Conductor Motion.* Palo Alto, CA: Electr. Power Res. Inst., 1979.
13. The thermal behavior of overhead conductors, *Electra,* **144**: 106–125, 1992.
14. *Calculation of bare overhead conductor temperature and ampacity under steady-state conditions,* ANSI/IEEE Std. 738, New York: American National Standards Institute, 1993.
15. P. H. Thomas, Sag calculations for suspended wires, *Trans. AIEE,* **30**: 2229, 1911.

16. J. P. Martin, *Sag Calculations by the Use of Martin's Tables.* Pittsburgh, PA: Copperweld Corp., 1931, revised 1961.
17. J. Bradbury, G. F. Kuska, and D. J. Tarr, Sag and tension calculations in mountainous terrain, *IEE Proc. C,* **129** (5): 213–220, 1982.
18. M. A. Uman, *The Lightning Discharge,* San Diego: Academic Press, 1987.
19. Working Group Report, Calculating the lightning performance of transmission lines, *IEEE Trans. Power Deliv.,* **5**: 1408–1417, 1990.
20. *Guide for application of gapped silicon-carbide surge arresters for alternating-current systems,* ANSI/IEEE Std. C62.2, New York: American National Standards Institute, 1987, revised 1995.
21. M. Zahn, *Electromagnetic Field Theory: A Problem Solving Approach,* Malabar, FL: Robert E. Krieger, 1987, pp. 96–103.
22. J. R. Carson, Wave propagation in overhead wires with ground return, *Bell Syst. Tech. J.,* **5**: 539–554, 1926.
23. M. Krakowski, Mutual impedance of crossing earth-return circuits, *Proc. IEE,* **114**: 253–257, 1967.
24. A. V. Mamishev and B. D. Russell, Measurement of magnetic fields in the direct proximity of power line conductors, *IEEE Trans. Power Deliv.,* **10**: 1211–1216, 1995.
25. J. Randa et al., Catalogue of electromagnetic environment measurements, 30–300 Hz, *IEEE Trans. Electromagn. Compat.,* **37**: 26–33, 1995.
26. *IEEE Standard Procedures for Measurement of Power Frequency Electric and Magnetic Fields from AC Power Lines,* ANSI-IEEE Std. 644-1987, New York: IEEE, 1987.
27. T. D. Bracken, Field measurements and calculations of electrostatic effects of overhead transmission lines, *IEEE Trans. Power Appar. Syst.,* **PAS-95**: 494–504, 1976.
28. C. J. Miller, The measurements of electric fields in live line working, *IEEE Trans. Power Appar. Syst.,* **PAS-86**: 493–498, 1967.
29. E. Weber, *Electromagnetic Theory,* New York: Dover, 1965, p. 131.
30. N. Wertheimer and E. Leeper, Electrical wiring configurations and childhood cancer. *Amer. J. Epidemiol.,* **109**: 273–284, 1979.
31. E. D. Sunde, *Earth Conduction Effects in Transmission Systems,* New York: Dover, 1968.
32. R. A. Walling, J. J. Paserba, and C. W. Burns, Series capacitor compensated shield scheme for enhanced mitigation of transmission magnetic fields, *IEEE Trans. Power Deliv.,* **8**: 461–469, 1993.
33. U. Jonsson, A. Larsson, and J. O. Sjodin, Optimized reduction of the magnetic field near Swedish 400 kV line by advanced control of shield wire currents, test results and economic evaluation, *IEEE Trans. Power Deliv.,* **9**: 961–969, 1994.
34. A. R. Memary and W. Janischewskyj, Mitigation of magnetic field near power lines, *IEEE Trans. Power Deliv.,* **11**: 1577–1586, 1996.
35. W. T. Kaune and L. E. Zaffanella, Analysis of magnetic fields produced far from electric power lines, *IEEE Trans. Power Deliv.,* **7**: 2082–2091, 1992.
36. P. Pettersson, Principles in transmission line magnetic field reduction, *IEEE Trans. Power Deliv.,* **11**: 1587–1593, 1996.

Reading List

H. M. Ryan (ed.), *High Voltage Engineering and Testing,* London: Peregrinus, 1994.

L. M. Faulkenberry and W. Coffer, *Electrical Power Distribution and Transmission,* Englewood Cliffs, NJ: Prentice-Hall, 1996.

A. J. Pansini, *Electrical Distribution Engineering,* 2nd ed., Lilburn, GA: Fairmont Press, 1992.

T. Gonen, *Electric Power Transmission System Engineering,* New York: Wiley, 1988.

W. L. Weeks, *Transmission and Distribution of Electrical Energy,* New York: Harper & Row, 1981.

B. M. Weedy, *Electric Power Systems,* 3rd ed., New York: Wiley, 1979.

EHV Transmission Line Reference Book, New York: Edison Electric Institute, 1968.

Electrical Transmission and Distribution Reference Book, 4th ed., East Pittsburgh, PA: Westinghouse Electric Corporation, 1964.

J. Zaborszky and J. W. Rittenhouse, *Electric Power Transmission.* New York: Ronald Press, 1954.

McDermott, T. E. Short, and J. G. Anderson, Lightning protection of distribution lines, *IEEE Trans. Power Deliv.,* **9**: 138–152, 1994.

ALEXANDER MAMISHEV
Massachusetts Institute of Technology